Available online at www.sciencedirect.com
ScienceDirect
Pattern Recognition 40 (2007) 705–717
PATTERN RECOGNITION
THE JOURNAL OF THE PATTERN RECOGNITION SOCIETY
www.elsevier.com/locate/patcog

# Extracting image orientation feature by using integration operator

Xudong Jiang*

*School of Electrical and Electronic Engineering, Nanyang Technological University, S1-B1c-109, 50 Nanyang Avenue, Singapore 639798, Singapore*

Received 24 October 2005; received in revised form 4 April 2006; accepted 21 April 2006

**Abstract**

This paper presents an orientation operator to extract image local orientation features. We show that a proper employment of image integration leads to an unbiased orientation estimate, based on which an orientation operator is proposed. The resulting discrete operator has flexibility in the scale selection as the scale change does not violate the bias minimization criteria. An analytical formula is developed to compare orientation biases of various discrete operators. The proposed operator shows lower bias than eight well-known gradient operators. Experiments further demonstrate higher orientation accuracy of the proposed operator than these gradient operators.


*Keywords:* Feature extraction; Image recognition; Gradient operator; Local orientation estimation; Orientation bias; Scale selection

## 1. Introduction

Orientation analysis appears in many different contexts in computer vision, image analysis, feature extraction and pattern recognition. Optical flow, fluid flow and some texture such as fingerprint and printed circuit board are typical oriented patterns. Edges and lines are important image features for both human perception and machine processing. Orientation analysis is widely employed in the edge and line detection, which is an important step in the object detection and recognition. Typical examples are the step and roof edge detector [1], the angular dispersion operator [2] and the Hermite transform method [3]. Local orientations play an important role in the texture analysis [4], optical flow [5] and oriented filter design [6,7]. They are crucial features for fingerprint classification [8–10] and matching [11,12].

Quite a lot of approaches were developed to extract the orientation feature. Early attempts were based on templates that could match ideal edge or line profiles [13–16]. Due to the variation of real edges and lines these methods often yield unreliable results. Other alternatives include matched-filter approaches [17,18] and spectral estimation methods [19]. However, the accuracy of the estimated orientation is limited by using these methods due to the limited number of fixed possible orientations. The well developed and most widely used approach for local orientation estimation is based on averaging squared gradients or principal component analysis of gradient covariance matrix. It was introduced in Refs. [20,21] and widely adopted by a large number of researchers for edge, corner and line detection [22–24], texture analysis [4,25], optical flow [5] and fingerprint recognition [26–29]. This prevalent local orientation estimation method consists of two components: gradient computation and squared-gradient averaging. While the gradient captures the orientation information at the pixel level, the averaging process attenuates noise contained in the gradient and therefore extracts smoothing local orientation features. Recently, problems of squared-gradient averaging were studied and an algorithm was proposed that captures the local dominant orientation more effectively by using a two-stage weighted average of the squared gradients [30].

Averaging the squared gradients can only reduce the estimation error caused by noise that has no dominant orientation in the average window. Anisotropic (oriented) noise can only be attenuated before the square operation, i.e., in the process of the gradient computation. There are two problems in the application of gradient for orientation estimation. One is the noise sensitivity as gradient inherently amplifies

* Tel.: +65 6790 5018; fax: +65 6793 3318.
*E-mail address:* exdjiang@ntu.edu.sg.

0031-3203/$30.00 
doi:10.1016/j.patcog.2006.04.028

the finer scale components (often noise) and suppresses the larger scale ones (often oriented pattern). The other is the orientation bias caused by the discrete operators that approximate to the differentiation. Many efforts were made to solve these two problems by designing various discrete operators. Pioneering attempts include Prewitt [31], Sobel, isotropic [14] and circular [32] operators. The well-known Canny operator [33] is approximated by the first Gaussian derivative $\nabla G$. Orientation of a certain scale can be robustly captured by the scale fitting of the Gaussian function. The pleasant properties of the $\nabla G$ operator were extensively discussed [34–37]. However, as we will see later, the $\nabla G$ operator produces high orientation bias if its scale deviates from the optimal one of a given operator size. The truncation of the Gaussian function to a finite operator size is one of the causes. Small operators are often preferred in many practical applications to preserve the image orientation locality and to reduce the computation load. Various finite-size discrete operators were therefore designed to minimize the orientation bias. Examples include the directional derivative (DD) operator [22], consistent operator [38] and optimal operator [39]. However, the scales of these operators are fixed for a given support size as all coefficients of operators are used up to approximate to the continuous gradient. There is thus no flexibility to alter the operator scale for the desired noise attenuation.

Unlike gradient operators that approximate to the differentiation, we propose an orientation operator that approximates to the integration to alleviate problems of orientation bias and scale flexibility. We first propose a continuous operator that works on a finite support region and prove its unbiased bandpass orientation computation in the next section. Scalable discrete operators are obtained by approximating to the integration in Section 3. To compare the proposed operator with others, Section 4 develops an analytical formula to compute orientation biases of various discrete operators. Section 5 further tests and compares various operators with some synthetic and real images. Conclusions are drawn in Section 6.

## 2. Proposed continuous orientation operator

For the local orientation estimation, we model the band-limited continuous image $f(x, y)$ locally as the sum of an oriented pattern and additive noise. In most practical applications, the oriented pattern can be approximated to have a constant orientation in a small local area within the operator window. Thus, an oriented image is locally modelled as

$$f(x, y) = h(x\cos\theta + y\sin\theta) + n(x, y), \tag{1}$$

where $h(t)$ is an arbitrary 1-D function ($h : \mathbb{R} \to \mathbb{R}$), $n(x, y)$ represents noise and $\theta + \pi/2$ is the local orientation of the oriented pattern, $-\pi/2 < \theta \leqslant \pi/2$.

The gradient can be represented by a complex variable as $\nabla f(x, y) = f_x(x, y) + jf_y(x, y)$ where $f_x(x, y)$ and $f_y(x, y)$ are the $x$- and $y$-differentials of image $f(x, y)$, respectively. For the oriented pattern (1) with $n(x, y) = 0$, we have $\nabla f(x, y) = \cos\theta h'(t) + j\sin\theta h'(t)$ with $h'(t) = \partial h(t)/\partial t$. We see that a non-zero gradient ($h'(t) \neq 0$) provides an unbiased orientation estimate (for $n(x, y)=0$), since $\mathrm{Im}[\nabla f(x, y)]/\mathrm{Re}[\nabla f(x, y)] = \tan\theta$. The transfer function from $f(x, y)$ to $\nabla f(x, y)$ is

$$T_\nabla(u, v) = 2\pi(-v + ju). \tag{2}$$

Obviously, it is a high-pass filter that amplifies the finer scale components and suppresses the larger scale ones. Another problem is the difficulty of the discrete approximation to the image differentiation. Large orientation error occurs if a simple finite difference is used to approximate to the differentiation.

One solution is to apply a low-pass filter and transfer the image differentiation to the derivative of the filter's impulse response. The Gaussian derivative operator is the most widely used example because of some excellent features of Gaussian function. However, the truncation of the filter to a finite size damages some desired properties of Gaussian function such as orientation isotropy. As orientation feature is captured by image differentiations, the limited operator size results in orientation error even for noise-free patterns because the derivative property of the operator is damaged by the truncation. A number of efforts [22,38,39] were made to approximate to the differentiation with size-limited discrete operator. Although these approaches use up all operator coefficients for the differentiation approximation and hence fix the operator scale, as we will see later, their orientation biases still do not reach the minimum. The roughening effect of the differentiation brings the difficulty of having an accurate discrete approximation.

To circumvent the inherent roughening effect of differentiation and the truncation problem of the derivative filter, this work proposes to use integration instead of differentiation to extract the orientation feature. As we will see below, a proper employment of integration achieves unbiased bandpass orientation estimation with a finite square-shape support region. It therefore circumvents problems of the limited operator size and the roughening effect of the differentiation.

The proposed continuous operator is defined as a weighted sum of $y$- and $x$-integrations in interval $2\Delta$ with shift $\Delta$ as

$$\mathscr{I}_R f(x, y) = \sum_{\Delta=-R}^{R} w_\Delta \left( \int_{y-\Delta}^{y+\Delta} f(x+\Delta, z)\,\mathrm{d}z + j\int_{x-\Delta}^{x+\Delta} f(z, y+\Delta)\,\mathrm{d}z \right), \tag{3}$$

in a finite square-shape support area of size $2R \times 2R$.

For the symbolic simplicity, let $\gamma(t) = \int h(t)\,\mathrm{d}t$, $\varepsilon = \Delta(\cos\theta + \sin\theta)$ and $\eta = \Delta(\cos\theta - \sin\theta)$. For the oriented

pattern (1) with $n(x, y) = 0$, Eq. (3) can be expressed as

$$\mathscr{I}_R f(x, y) = \sum_{\Delta=-R}^{R} w_\Delta \left[ \frac{\gamma(t+\varepsilon) - \gamma(t+\eta)}{\sin\theta} + j\frac{\gamma(t+\varepsilon) - \gamma(t-\eta)}{\cos\theta} \right], \quad (4)$$

where $t = x\cos\theta + y\sin\theta$. With the constraint of $w_{-\Delta} = w_\Delta$, it is not difficult to rewrite Eq. (4) as

$$\mathscr{I}_R f(x, y) = (\cos\theta + j\sin\theta) \sum_{\Delta=0}^{R} w_\Delta \times \frac{\gamma(t+\varepsilon) - \gamma(t+\eta) + \gamma(t-\varepsilon) - \gamma(t-\eta)}{\sin\theta\cos\theta}. \quad (5)$$

We see that the non-zero $\mathscr{I}_R f(x, y)$ provides an unbiased orientation estimate independent of $R$, $\Delta$ and $w_\Delta$, since

$$\frac{\mathrm{Im}[\mathscr{I}_R f(x, y)]}{\mathrm{Re}[\mathscr{I}_R f(x, y)]} = \tan\theta. \quad (6)$$

By using the translation property of the Fourier transform, it is not difficult to obtain the transfer function from $f(x, y)$ to $\mathscr{I}_R f(x, y)$ as

$$T_{\mathscr{I}_R}(u, v) = \frac{2(-v + ju)}{\pi u v} \sum_{\Delta=0}^{R} w_\Delta \sin(2\pi\Delta u)\sin(2\pi\Delta v). \quad (7)$$

Obviously, it is a bandpass filter comparing to the high-pass filter of the gradient (2).

Unlike gradient that amplifies the finer scale components (often noise) and suppresses the larger scale ones (often oriented pattern), the proposed operator provides an unbiased bandpass orientation estimate with the flexibility of scale selection by choosing the free parameter $w_\Delta$. The optimal scale match between the operator and the oriented pattern maximizes the noise reduction and therefore minimizes the orientation estimation error caused by noise. Moreover, the proposed operator facilitates unbiased bandpass orientation estimation using a finite square-shape support region. This circumvents the problem of size limited square-shape operator window in the practical applications. In addition, the discrete approximation to integration is in general more stable than that to differentiation because it is well known that the smoothness properties deteriorate in the process of differentiation [40]. Therefore, it is expected that the discrete version of the proposed operator is able to achieve lower orientation bias than various gradient operators. This will be demonstrated in the subsequent sections.

## 3. Proposed discrete orientation operator

The proposed discrete orientation operator is a discrete approximation to the continuous operator (3) presented in the last section. We consider the discrete image $\mathfrak{f}(k, l)$ sampled from a continuous image $f(x, y)$ as $\mathfrak{f}(k, l) = f(kT, lT)$. By choosing $\Delta = iT$ or $\Delta = (i + 0.5)T$, $i \in \mathbb{Z}$, respectively, for operators centered at a pixel or at the middle point of four nearest pixels, we can obtain the discrete version of the operator (3) by only approximating to the 1-D integrations. Numeric quadrature formulae [41] such as the well-known Newton–Cotes formulae can be applied to compute numeric integration using sample points within the integration interval. However, the operator (3) contains integrations in the intervals $2\Delta$ where $|\Delta| < R$. To fully make use of the data within the $2R \times 2R$ operator window, we shall use data outside the integration interval as well for more accurate approximation. Therefore, we present the discrete approximation to the integration from the interpolation of the discrete function, with which data outside the integration interval are also used in the approximation.

We first approximate an unknown continuous integrand function $r(t)$ at intermediate $t$-values, $t \neq t_0 + iT$ by an interpolation polynomial that passes through the known sample points $r_i = r(t_0 + iT)$, $i = 0, 1, 2, \ldots, M$, as

$$r(t) \approx P_M(t) = \sum_{i=0}^{M} r_i \phi_i^M(t), \quad (8)$$

where the $M + 1$ functions $\phi_i^M(t)$ are $M$th degree polynomials. Letting $t = t_0 + sT$, the Lagrange interpolation coefficients $\phi_i^M(t)$ [41] are expressed as

$$\phi_i^M(t) = \frac{(-1)^{M-i}}{M!} \binom{M}{i} \prod_{b=0, b\neq i}^{M} (s - b), \quad (9)$$

where $b \in \mathbb{Z}$.

The integration of an unknown continuous integrand function $r(t)$ is approximated by the integration of its interpolation polynomial $P_M(t)$. Substituting Eq. (9) into Eq. (8) yields

$$\int_{t_p}^{t_q} r(t)\,\mathrm{d}t \approx \int_{t_p}^{t_q} P_M(t)\,\mathrm{d}t = \sum_{i=0}^{M} r_i \frac{(-1)^{M-i}}{M!} \binom{M}{i} T \times \int_{s_p}^{s_q} \prod_{b=0, b\neq i}^{M} (s - b)\,\mathrm{d}s, \quad (10)$$

where $s = (t - t_0)/T$, $s_p = (t_p - t_0)/T$, $s_q = (t_q - t_0)/T$ and $0 \leqslant s_p, s_q \leqslant M$. Obviously, Eq. (10) is a weighted sum of $r_i$. Given $M$, $s_p$ and $s_q$, the weights denoted by $h_i^M(s_p, s_q)$ are computed by (ignoring the constant $T$)

$$h_i^M(s_p, s_q) = \frac{(-1)^{M-i}}{M!} \binom{M}{i} \int_{s_p}^{s_q} \prod_{b=0, b\neq i}^{M} (s - b)\,\mathrm{d}s. \quad (11)$$

Applying Eq. (10) with the integration interval $t_q - t_p = 2\Delta$, the polynomial degree $M = 2R/T$ and $i = m + M/2$ to

Eq. (3), we obtain the discrete version of Eq. (3) as

$$\mathscr{J}_M\tilde{f}(k,l) = \sum_{n=-M/2}^{M/2} w_n \sum_{m=-M/2}^{M/2} g_{m,n}^M [\tilde{f}(k+n, l+m) + j\tilde{f}(k+m, l+n)], \quad (12)$$

where $n = \Delta/T$. Letting $m_- = M/2 - m$, $m_+ = M/2 + m$, $n_- = M/2 - n$ and $n_+ = M/2 + n$ for symbolic simplicity, the weights $g_{m,n}^M$ are obtained from Eq. (11) as

$$g_{m,n}^M = h_{m_+}^M(n_-, n_+) = \frac{(-1)^{m_-}}{m_-!m_+!} \int_{n_-}^{n_+} \prod_{b=0, b\neq m_+}^{M} (s-b)\,\mathrm{d}s, \quad (13)$$

where $\{M, m_-, m_+, n_-, n_+, b\} \in \mathbb{Z}$. From Eq. (13) it is easy to prove that $g_{-m,n}^M = g_{m,n}^M$ and $g_{m,-n}^M = -g_{m,n}^M$. This means that we need only tabulate the values of $g_{m,n}^M$ for $m \geqslant 0$ and $n > 0$. Table 1 shows $g_{m,n}^M$ computed by Eq. (13) for $M$ from 2 to 7.

Formula (12) with the fixed coefficients $g_{m,n}^M$ computed by Eq. (13) and a free parameter $w_n$ is our proposed discrete orientation operator $\{o_{m,n}^M\} = \{w_n g_{m,n}^M\}$ of size $(M+1) \times (M+1)$. For example, the $4 \times 4$ and $5 \times 5$ operators with $w_n \equiv 1$ can be obtained from Table 1 as

$$\begin{bmatrix} -0.3750 & -1.1250 & -1.1250 & -0.3750 \\ 0.0417 & -0.5417 & -0.5417 & 0.0417 \\ -0.0417 & 0.5417 & 0.5417 & -0.0417 \\ 0.3750 & 1.1250 & 1.1250 & 0.3750 \end{bmatrix} \quad \text{and}$$

$$\begin{bmatrix} -0.3111 & -1.4222 & -0.5333 & -1.4222 & -0.3111 \\ 0.0111 & -0.3778 & -1.2667 & -0.3778 & 0.0111 \\ 0 & 0 & 0 & 0 & 0 \\ -0.0111 & 0.3778 & 1.2667 & 0.3778 & -0.0111 \\ 0.3111 & 1.4222 & 0.5333 & 1.4222 & 0.3111 \end{bmatrix}.$$

The parameter $w_n$ is used to change the operator's scale or frequency selection, which does not violate the optimizing regularization of the unbiased orientation estimation. Thus, the weights $w_n$ provide us freedom to control the operator scale. This feature is very useful because the scale match between the operator and the oriented pattern maximizes the noise reduction and therefore minimizes the orientation estimation error caused by noise. In general, we can choose any $w_n$ ($w_n \in \mathbb{R}^+$) with $w_{-n} = w_n$ to achieve a desired scale for a specific application. While not limiting ourselves from other possible choices, we use a Gaussian function $w_n = \exp(-n^2/2\sigma^2)$ in this work so that we can easily adjust the operator scale by varying $\sigma$ only.

## 4. Characteristics of the discrete operators

There are two error sources of the orientation estimation if discrete operators are employed. One is the orientation bias caused by the finite operator size and discrete approximation to the continuous function, which occurs even for a noise-free oriented pattern. The other is noise which needs to be attenuated by scale fitting of the operator to the oriented pattern. In this section we compare various discrete operators based on their scales and orientation biases.

Table 1
Proposed discrete orientation operator coefficients $g_{m,n}^M$ of various orders $M$ for $m \geqslant 0$ and $n > 0$

| $M$ | $n$ | $m = 0/0.5$ | $m = 1/1.5$ | $m = 2/2.5$ | $m = 3/3.5$ |
|---|---|---|---|---|---|
| 2 | 1 | 1.3333 | 0.3333 | | |
| 3 | 0.5 | 0.5417 | −0.0417 | | |
| | 1.5 | 1.1250 | 0.3750 | | |
| 4 | 1 | 1.2667 | 0.3778 | −0.0111 | |
| | 2 | 0.5333 | 1.4222 | 0.3111 | |
| 5 | 0.5 | 0.5569 | −0.0646 | 0.0076 | |
| | 1.5 | 1.0875 | 0.4312 | −0.0187 | |
| | 2.5 | 0.8681 | 1.3021 | 0.3299 | |
| 6 | 1 | 1.2402 | 0.3976 | −0.0190 | 0.0013 |
| | 2 | 0.7026 | 1.2952 | 0.3619 | −0.0085 |
| | 3 | 1.9429 | 0.1929 | 1.5429 | 0.2929 |
| 7 | 0.5 | 0.5648 | −0.0788 | 0.0155 | −0.0016 |
| | 1.5 | 1.0730 | 0.4574 | −0.0333 | 0.0029 |
| | 2.5 | 0.9249 | 1.1998 | 0.3867 | −0.0114 |
| | 3.5 | 1.2108 | 0.5359 | 1.4490 | 0.3042 |

The operator's scale represented by the transfer function can be obtained by the discrete Fourier transform of the operator. As the transfer functions of all discrete gradient operators are bandpass filters, we divide them by the transfer function of true gradient $2\pi(-v + ju)$ and call the quotients pre-filter. It is easier to compare them by their bandwidths since pre-filters of all operators are low-pass filters.

We have not found any analytical formula in literature that calculates the orientation bias of discrete operators. As different operators were designed by different criteria, it is helpful to develop some means of bias computation to assess various operators. Orientation bias is defined by the difference between the true orientation and the expectation of its estimates. The expectation is measured by the ensemble average over all possible states of a noise-free pattern with the same constant orientation within the operator window. Since orientation has period of $\pi$ and discontinuity at $\pm\pi/2$ and the phase of the operator's output has period of $2\pi$, the direct average of orientations or operator's outputs is problematic. A solution is to average the squared outputs of the operator. It has been proven in Ref. [29] that the squared gradient average leads to the same result as that of the orientation tensor or principal component analysis of gradient covariance matrix. The half angle of the average squared output of an operator represents the expectation of its orientation estimates.

The output of applying an orientation operator $\{o^M_{m,n}\}$ to a discrete image $\mathfrak{f}(k,l)$ can be expressed as

$$\mathcal{O}_M\mathfrak{f}(k,l) = \sum_{n=-M/2}^{M/2}\sum_{m=-M/2}^{M/2} o^M_{m,n}[\mathfrak{f}(k+n,l+m) + j\mathfrak{f}(k+m,l+n)]. \quad (14)$$

The ensemble average of $(\mathcal{O}_M\mathfrak{f}(k,l))^2$ over all possible states of $\mathfrak{f}(k,l)$ is expressed as

$$E_{\mathfrak{f}}[(\mathcal{O}_M\mathfrak{f}(k,l))^2] = E_{\mathfrak{f}}[A^2(k,l)] - E_{\mathfrak{f}}[B^2(k,l)] + 2jE_{\mathfrak{f}}[A(k,l)B(k,l)], \quad (15)$$

where

$$A(k,l) = \sum_{n=-M/2}^{M/2}\sum_{m=-M/2}^{M/2} o^M_{m,n}\mathfrak{f}(k+n,l+m), \quad (16)$$

$$B(k,l) = \sum_{n=-M/2}^{M/2}\sum_{m=-M/2}^{M/2} o^M_{m,n}\mathfrak{f}(k+m,l+n). \quad (17)$$

For a noise-free pattern with constant orientation within the operator window $\mathfrak{f}(k,l) = h(k\cos\theta + l\sin\theta)$, Eq. (16) can be rewritten as

$$A(k,l) = A_1(t) = \sum_{n=-M/2}^{M/2}\sum_{m=-M/2}^{M/2} o^M_{m,n} \times h(t + n\cos\theta + m\sin\theta), \quad (18)$$

where $A_1(t)$ and $h(t)$ are 1-D functions and $t = k\cos\theta + l\sin\theta$.

As $h(t)$ goes through all states of a noise-free pattern $\mathfrak{f}(k,l)$ with $t$ varying form $-\infty$ to $\infty$, we can use the average over $t$ to replace the ensemble average over $\mathfrak{f}$. Based on Parseval's Theorem we have

$$E_{\mathfrak{f}}[A^2(k,l)] = \sum_{t=-\infty}^{\infty} A_1^2(t) = \frac{1}{2\pi}\int_{-\pi}^{\pi} |\mathfrak{A}(\omega)|^2\,\mathrm{d}\omega, \quad (19)$$

where $\mathfrak{A}(\omega)$ is the Fourier transform of $A_1(t)$.

Using the translation property of the Fourier transform and the symmetry property of $o^M_{m,n}$ ($o^M_{-m,n} = o^M_{m,n}$, $o^M_{m,-n} = -o^M_{m,n}$), it is not too difficult to have

$$\mathfrak{A}(\omega) = 2jH(\omega)\sum_{m=e}^{M/2}\sum_{n=e}^{M/2}\alpha_m o^M_{m,n} \times \cos(\omega m\sin\theta)\sin(\omega n\cos\theta), \quad (20)$$

where $H(\omega)$ is the Fourier transform of $h(t)$, $\alpha_0 = 1$ and $\alpha_m = 2$ for $m > 0$. $e = 0.5$ and 0, respectively, for odd and even numbers of $M$. $\{m,n\} - e \in \mathbb{Z}$.

If we denote the sum term in Eq. (20) by $G^M_\omega(\sin\theta,\cos\theta)$, i.e.

$$G^M_\omega(\sin\theta,\cos\theta) = \sum_{m=e}^{M/2}\sum_{n=e}^{M/2}\alpha_m o^M_{m,n} \times \cos(\omega m\sin\theta)\sin(\omega n\cos\theta), \quad (21)$$

we have $\mathfrak{A}(\omega) = 2jH(\omega)G^M_\omega(\sin\theta,\cos\theta)$.

Similarly, we have $\mathfrak{B}(\omega) = 2jH(\omega)G^M_\omega(\cos\theta,\sin\theta)$, where

$$G^M_\omega(\cos\theta,\sin\theta) = \sum_{m=e}^{M/2}\sum_{n=e}^{M/2}\alpha_m o^M_{m,n} \times \cos(\omega m\cos\theta)\sin(\omega n\sin\theta). \quad (22)$$

Thus, the orientation bias $b_M$ of a discrete operator is computed by

$$b_M = \frac{1}{2}\tan^{-1}\frac{2\int_{-\pi}^{\pi}|H(\omega)|^2 G^M_\omega(\sin\theta,\cos\theta)G^M_\omega(\cos\theta,\sin\theta)\,\mathrm{d}\omega}{\int_{-\pi}^{\pi}|H(\omega)|^2[{G^M_\omega}^2(\sin\theta,\cos\theta) - {G^M_\omega}^2(\cos\theta,\sin\theta)]\,\mathrm{d}\omega} - \theta. \quad (23)$$

For a single frequency oriented pattern, the bias is simply computed by

$$b_M = \frac{1}{2}\tan^{-1}\frac{2G^M_\omega(\sin\theta,\cos\theta)G^M_\omega(\cos\theta,\sin\theta)}{{G^M_\omega}^2(\sin\theta,\cos\theta) - {G^M_\omega}^2(\cos\theta,\sin\theta)} - \theta. \quad (24)$$

The developed formulae (23) and (24) can be used to compute the orientation bias of any discrete operator $\{o^M_{m,n}\}$ as long as it extracts the orientation feature by the phase of the output of Eq. (14) and holds the symmetry property ($o^M_{-m,n} = o^M_{m,n}$, $o^M_{m,-n} = -o^M_{m,n}$). Orientation biases of all nine operators used in the comparison of this paper can be computed by Eq. (23) or (24).

We first compare the proposed $3\times 3$ operator with the well-known Prewitt [31], isotropic [14], Sobel, circular [32], optimal [39] and consistent [38] operators. All of them except Prewitt operator were designed based on some criteria of isotropy, circularity, orientation invariance and consistency. In addition, a $3\times 3$ Gaussian derivative operator $\nabla G$ with suggested $\sigma = 0.5$ in Refs. [34,38] is also included in the comparison. The pre-filters' transfer characteristics of these operators are illustrated in Fig. 1a. Their average radial bandwidths over all directions are recorded in Table 2. They range from 0.202 to 0.238. According to the maximal bandwidth, the test oriented patterns are chosen to have unity power spectrum in (0, 0.238] and zero outside. Fig. 1b plots the orientation estimation biases of the above operators against the true orientations of the test patterns computed by Eq. (23). Table 2 records the maximal biases (over all true orientations) in degree. Fig. 1b and Table 2 demonstrate that our proposed $3\times 3$ operator achieves the lowest orientation estimation bias by a significant margin.

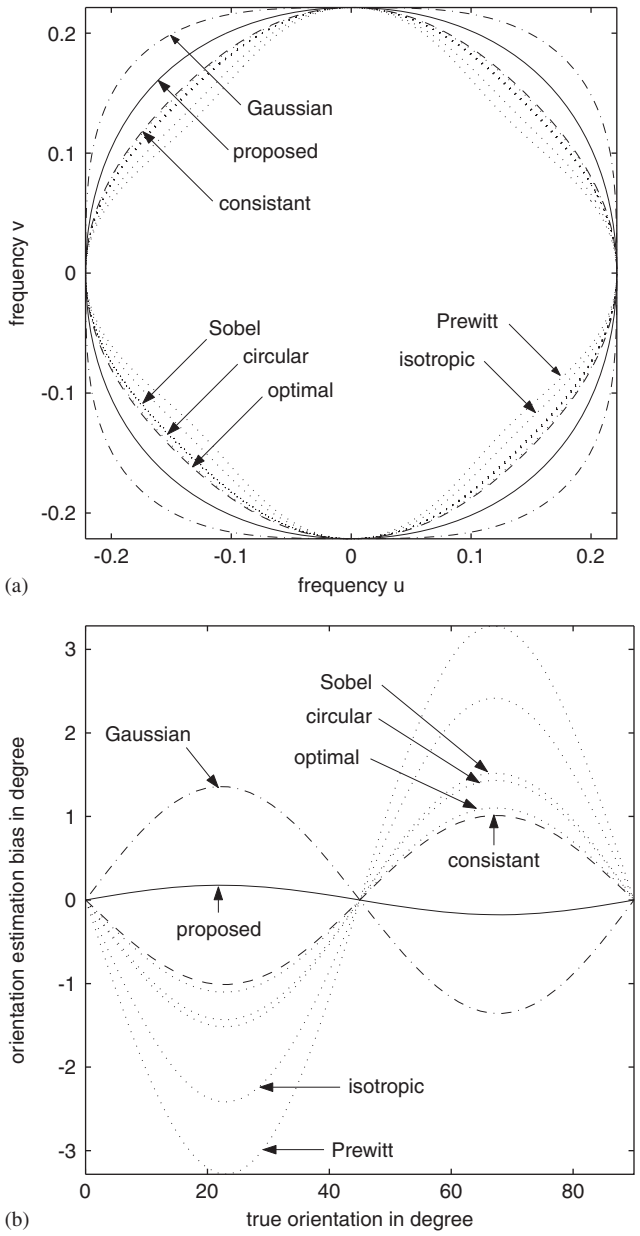


Fig. 1. Pre-filters' transfer characteristics of various $3 \times 3$ operators and their orientation estimation biases. (a) Contours of height 0.5 of the square amplitude transfer function, (b) biases against the true orientation computed by Eq. (23).

The bandwidths of the $5 \times 5$ consistent, optimal and DD [22] operators and the $7 \times 7$ optimal and DD operators are 0.150, 0.149, 0.163 and 0.124, 0.129, respectively. According to the maximum bandwidths, the test oriented patterns are chosen to have unity power spectrum in (0, 0.163] and (0 0.129] for the $5 \times 5$ and $7 \times 7$ operators, respectively, and zero outside. Fig. 2 plots the pre-filters' characteristics of the optimal and DD operators. We do not plot the consistent operator since it is very close to the optimal operator and the maximal operator size given in Ref. [38] is $5 \times 5$. The proposed and $\nabla G$ operators larger than $3 \times 3$ are scalable. For the $5 \times 5$ $\nabla G$ operator, $\sigma = 0.8$ and 0.96 were suggested in Refs. [34,38,39], respectively. For the $7 \times 7$ $\nabla G$ operator, $\sigma = 1.12$ was suggested in Ref. [39]. We test the $5 \times 5$ $\nabla G$ operator with five different $\sigma$ values (0.55, 0.8, 0.96, 1.25 and 1.55) and the $7 \times 7$ $\nabla G$ operator with $\sigma$ values of 0.6, 0.95, 1.12, 1.7 and 2.3. For comparison, we choose the $\sigma$ values of the proposed operators that lead to the same bandwidths as those of the $\nabla G$ operators, respectively. For these two scalable operators, Fig. 2 plots their pre-filters' characteristics of the smallest and the largest scales used in the test. Table 2 numerically records the maximal orientation estimation biases (over all true orientations) of various operators computed by Eq. (23) and the pre-filters' bandwidths. The $\sigma$ values used for the two scalable operators are also indicated in Table 2.

Table 2 demonstrates that the proposed operators achieve the lowest orientation estimation biases for all tested scales. The highest bias of the proposed operator is lower than the lowest bias of all other operators. Moreover, the highest bias of the proposed $5 \times 5$ operator is even lower than the lowest bias of all other $7 \times 7$ operators. We see that the bias of the $\nabla G$ operator is very sensitive to the $\sigma$ value. The scale flexibility of the $\nabla G$ operator is therefore at a price of the high orientation bias. In contrast to that and the fixed scale of other operators, a conspicuous advantage of the proposed operator is that it keeps low bias for various different scales. This facilitates an accurate and noise robust orientation estimate by adjusting its scale freely without sacrificing the low orientation bias. The optimal scale fitting between the operator and the oriented pattern maximizes the noise reduction and therefore minimizes the orientation estimation error caused by noise.

For the application of pre-designed operators in an online system, the computational consumption is an important issue. For symbolic simplicity, we consider the even number $N$ of an $N \times N$ symmetric operator, which has $N^2/4$ different absolute values of coefficients. For efficient computation, we first add/subtract the four image pixels that have the same absolute coefficient value. The $3N^2/4$ arithmetic operations produce $N^2/4$ pixel sums, which are multiplied by the corresponding operator coefficients. Finally, $N^2/4 - 1$ additions compute the real or imaginary part of the operator's output. For the multi-scale processing, if $q$ outputs using the same operator size but different scales are to be computed, we need

$$C_c^N(q) = 3N^2/4 + q(N^2/4 + N^2/4 - 1)$$
$$= 3N^2/4 + q(N^2/2 - 1) \quad (25)$$

arithmetic operations for conventional operators, $q \geqslant 1$. This is because the scale change results in changes of all operator coefficients in general. For the proposed operator, however, $g_{m,n}^{N-1}$ is fixed and the scale is adjusted by varying $w_n$ only. Therefore, after the $3N^2/4$ pixel additions, we need $N^2/4$ multiplications for only once. Then, $N/2$ results

Table 2
Pre-filters bandwidths and orientation estimation biases of various operators

| 3 × 3 | Bandwidth | Bias | 5 × 5 | Bandwidth | Bias | 7 × 7 | Bandwidth | Bias |
|---|---|---|---|---|---|---|---|---|
| Consistent | 0.215 | 1.0120 | Consistent | 0.150 | 0.0573 | – | – | – |
| Optimal | 0.214 | 1.1024 | Optimal | 0.149 | 0.0829 | Optimal | 0.124 | 0.0102 |
| – | – | – | DD | 0.163 | 0.0990 | DD | 0.129 | 0.2802 |
| ∇G(0.5) | 0.238 | 1.3585 | ∇G(0.55) | 0.225 | 0.3858 | ∇G(0.60) | 0.213 | 0.1174 |
| Prewitt | 0.202 | 3.2827 | ∇G(0.80) | 0.168 | 0.0785 | ∇G(0.95) | 0.139 | 0.0189 |
| Isotropic | 0.206 | 2.4173 | ∇G(0.96) | 0.147 | 0.3759 | ∇G(1.12) | 0.121 | 0.1201 |
| Circular | 0.212 | 1.4327 | ∇G(1.25) | 0.130 | 1.1926 | ∇G(1.70) | 0.094 | 1.2845 |
| Sobel | 0.212 | 1.5178 | ∇G(1.55) | 0.124 | 2.6574 | ∇G(2.30) | 0.086 | 2.4305 |
| Proposed | 0.225 | 0.1766 | pro.(0.42) | 0.225 | 0.0032 | pro.(0.59) | 0.213 | 0.0001 |
| – | – | – | pro.(0.81) | 0.168 | 0.0005 | pro.(0.92) | 0.139 | 0.0000 |
| – | – | – | pro.(1.00) | 0.147 | 0.0030 | pro.(1.15) | 0.121 | 0.0001 |
| – | – | – | pro.(1.58) | 0.130 | 0.0061 | pro.(1.93) | 0.094 | 0.0002 |
| – | – | – | pro.(4.26) | 0.124 | 0.0076 | pro.(5.94) | 0.086 | 0.0004 |

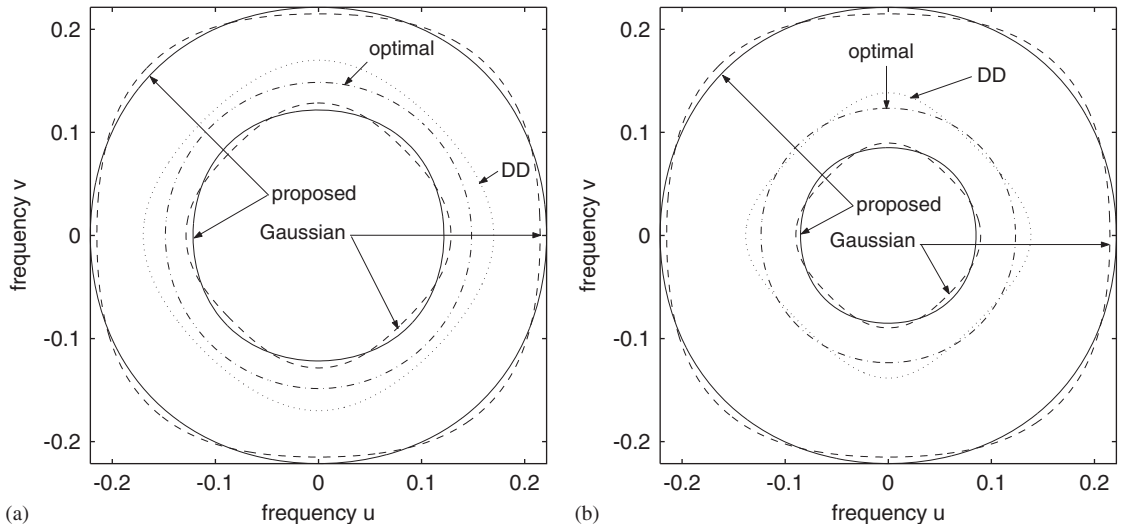


Fig. 2. Pre-filters' transfer characteristics of various operators. Contours of height 0.5 of the square amplitude transfer functions for (a) 5 × 5 and (b) 7 × 7 operators. The smaller/larger circles of the proposed and ∇G operators are for the largest/smallest scales used in the test.

corresponding to the same $w_n$ are summed together for each of the $N/2$ different $w_n$ so that $N/2(N/2-1)=N(N-2)/4$ additions are needed, again for only once. Finally, for each of the $q$ scales, $N/2$ multiplications and $N/2-1$ additions compute the real or imaginary part of the operator's output. As a result, we need

$$\begin{aligned} C_p^N(q) &= 3N^2/4 + N^2/4 + N(N-2)/4 \\ &\quad + q(N/2 + N/2 - 1) \\ &= 5N^2/4 - N/2 + q(N-1) \end{aligned} \tag{26}$$

arithmetic operations for $q > 1$. Note that $C_p^N(1) = C_c^N(1)$ because $\{w_n g_{m,n}^{N-1}\}$ can be pre-computed for the single scale application. Fig. 3 shows the number of arithmetic operations against the number of scales calculated by Eq. (25) and (26) for the conventional and proposed operators. The computational efficiency of the proposed operator for the multiscale processing is visible from Fig. 3.

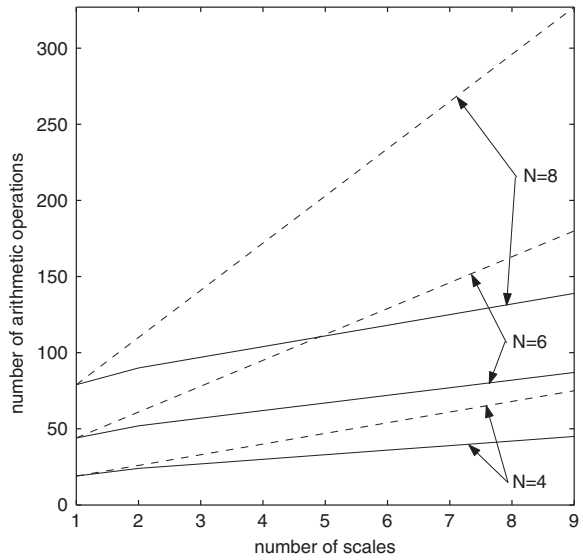


Fig. 3. Number of arithmetic operations against the number of scales for the proposed (solid line) and conventional (dashed line) operators of size $N \times N$.

## 5. Experiments

### 5.1. Testing with synthetic images

A 256 × 256 Fresnel pattern shown in Fig. 4a and a 220 × 512 image consisting of a step edge with the orientation of 22.5° are generated. The Fresnel pattern has all possible, variable orientations and a wide frequency range. The step edge has the gray value of $d$ in one edge side and $-d$ in the other side. Its power spectrum spreads over the whole frequency range. Gaussian white noise with standard deviation $\sigma_n$ is used to contaminate test images. Fig. 4b shows a sample image of the contaminated Fresnel pattern.

Images are divided into blocks of size $9 \times 9$ and the dominant orientation of each block is computed by the average of the squared operator outputs in the block. For Fresnel pattern, orientations of all blocks except the innermost four are used in the accuracy test. For the step edge, orientation of the block most close to the edge in each block row is selected for test. We test the estimation accuracy for noise-free, lighter- and heavier-contaminated images. The lighter contaminated images have signal-to-noise ratio of 9 db for Fresnel pattern and $d/\sigma_n = 4$ for step edge. The heavier contaminated images have signal-to-noise ratio of 0 db for Fresnel pattern and $d/\sigma_n = 2$ for step edge. We calculate the mean square root of the estimation errors and record it in Table 3.

Table 3 shows that the proposed 3 × 3 operator achieves the smallest orientation estimation errors among all 3 × 3 operators for the step edges with all the three different noise levels. Although the proposed $3 \times 3$ operator outperforms all other 3 × 3 operators by a significant margin for the noise-free Fresnel pattern, it has the second largest errors for the contaminated ones due to its second largest bandwidth (see Fig. 1a and Table 2). The proposed 3 × 3 operator is not scalable as we have only $w_1 = w_{-1}$. Varying the value of $w_1$ does not change the operator scale.

For the proposed and $\nabla G$ operators of size 5 × 5 and 7 × 7, we apply different values of scale $\sigma$ to the heavy contaminated images and choose the $\sigma$ values that achieve the minimal orientation error. Table 3 records the orientation estimation errors of various operators and the corresponding $\sigma$ values. It shows that the proposed $5 \times 5$ and $7 \times 7$ operators achieve the smallest orientation estimation errors compared to all other operators of the same size for both the oriented patterns and all three different noise levels.

### 5.2. Testing with real images

Two real fingerprints, one of which has good and the other bad quality shown in Fig. 5, are used for testing. The dominant orientation of each 9 × 9 image block is estimated by the average squared operator output in the block. As the true local orientations of a real image are unknown, we rotate each image block by 45° and then estimate its dominant orientation again. The difference between the two orientation estimates should be 45° in expectation. However, it usually deviates from 45° due to the different biases at different true orientations (see Fig. 1b). Furthermore, the original and rotated blocks have some different pixels due to the square shape of the block, which also affects the orientation difference. Therefore, the deviation of the orientation difference from the rotation angle indirectly reflects the operator's bias and noise robustness. The mean square root of the deviations (in degree) over the fingerprint is shown in Table 4. We call it indirect error to differentiate it from the error against the true orientation.

Table 4 shows that the proposed 3 × 3 operator outperforms all other operators for the good fingerprint. For the bad fingerprint, it has higher indirect error than some other operators due to its wider bandwidth. For the proposed and $\nabla G$ operators of size 5 × 5 and 7 × 7, various different $\sigma$ values are tested to find the best scales that achieve the minimal errors. The best scales of the proposed (5 × 5)/(7 × 7)

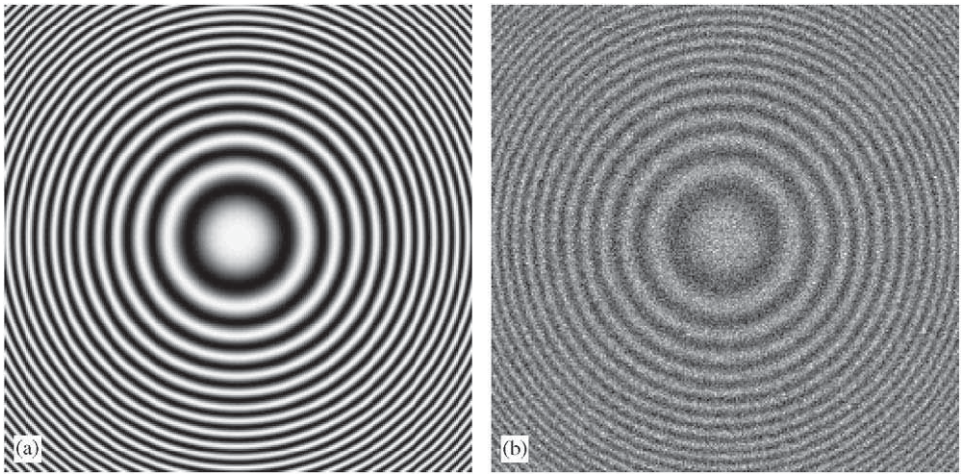


Fig. 4. (a) A Fresnel pattern and (b) its noisy version.

Table 3
Mean square root of orientation estimation errors in degree of various operators

| Operator, | Error for Fresnel pattern | | | Error for step edge | | |
|---|---|---|---|---|---|---|
| $\sigma$ for Fresnel/step edge | Noise free | S/N = 9 db | S/N = 0 db | Noise free | $d/\sigma_n = 4$ | $d/\sigma_n = 2$ |
| Prewitt $3 \times 3$ | 1.6069 | 2.3197 | 10.0446 | 3.0777 | 3.7534 | 4.8401 |
| Isotropic $3 \times 3$ | 1.1817 | 2.1951 | 10.1499 | 2.4937 | 3.0871 | 4.0973 |
| Sobel $3 \times 3$ | 0.7486 | 2.2680 | 10.8916 | 1.8925 | 2.3972 | 3.3702 |
| Circular $3 \times 3$ | 0.7082 | 2.2855 | 10.9497 | 1.8401 | 2.33523 | 3.3072 |
| Consistent $3 \times 3$ | 0.5102 | 2.3978 | 11.3040 | 1.6087 | 2.0500 | 3.0224 |
| Optimal $3 \times 3$ | 0.5526 | 2.3704 | 11.2219 | 1.6783 | 2.1079 | 3.0796 |
| $\nabla G$ $3 \times 3$, $\sigma = 0.5$ | 0.6217 | 3.6955 | 12.4320 | 2.5353 | 2.5028 | 3.3854 |
| Proposed $3 \times 3$ | 0.1267 | 2.9258 | 11.7633 | 1.5131 | 1.7037 | 2.6631 |
| Consistent $5 \times 5$ | 0.1192 | 1.2168 | 6.9815 | 1.0412 | 1.4448 | 2.2308 |
| Optimal $5 \times 5$ | 0.1315 | 1.2046 | 6.8911 | 1.0292 | 1.4376 | 2.2220 |
| DD $5 \times 5$ | 0.1860 | 1.2899 | 7.4251 | 1.0070 | 1.5138 | 2.4389 |
| $\nabla G$ $5 \times 5$, $\sigma = 1.43/1.04$ | 1.9831 | 2.2448 | 5.2850 | 1.0331 | 1.4744 | 2.2406 |
| Proposed $5 \times 5$, $\sigma = 4.3/4.3$ | 0.1118 | 1.0054 | 5.1022 | 0.8232 | 1.2573 | 2.0047 |
| Optimal $7 \times 7$ | 0.1262 | 1.1166 | 5.1354 | 0.8940 | 1.4227 | 2.3232 |
| DD $7 \times 7$ | 0.9671 | 1.7227 | 6.0237 | 0.9403 | 1.4234 | 2.2757 |
| $\nabla G$ $7 \times 7$, $\sigma = 1.48/1.57$ | 1.2308 | 1.5802 | 4.1259 | 0.9709 | 1.3431 | 2.0739 |
| Proposed $7 \times 7$, $\sigma = 3.37/6$ | 0.1184 | 0.9537 | 3.3378 | 0.5364 | 1.1321 | 1.9899 |

Fig. 5. Two fingerprints with good (left) and bad (right) quality.

operators are 4.3/2.8 and 4.3/6, respectively, for the good and bad fingerprints. Those of the $\nabla G$ operators are 0.920/1.179 and 1.170/1.512. To study the orientation estimation error with unmatched scales, we test operators with scales $\sigma$ deviating from their best ones $\sigma_m$. The proposed operators with scales $\sigma_m/2$ and $2\sigma_m$ and the $\nabla G$ operators with scales $\sigma_m/\sqrt{2}$ and $\sqrt{2}\sigma_m$ are tested. Their results are marked with signs $-$ and $+$, respectively, in Table 4. It shows that the proposed $5 \times 5$ and $7 \times 7$ operators, even with the scale parameter that is half or two times of the best fitting one, achieve the lowest indirect errors compared with all other operators of the same size for both the real fingerprints. In contrast to that, the $\nabla G$ operator performs badly if its scale is not properly selected. This demonstrates again the superiority of the proposed operators in respect of the orientation accuracy and the scale flexibility.

To test the computational cost, orientation vectors of all pixels of the above $240 \times 270$ images were computed by a C program executed under Windows XP Professional O.S. on a HP xw4100 (Intel Pentium 4 at 3.0 GHz) PC. The average processing time of $7 \times 7$ operators over 1000 images was recorded. For the single-scale application, all operators took

Table 4
Deviation of orientation difference from the rotation angle caused by various operators

| $3 \times 3$ | G. im. | B. im. | $5 \times 5$ | G. im. | B. im. | $7 \times 7$ | G. im. | B. im. |
|---|---|---|---|---|---|---|---|---|
| Consistent | 1.8085 | 9.1493 | Consistent | 1.5794 | 8.6014 | – | – | – |
| Optimal | 1.8467 | 9.1675 | Optimal | 1.5986 | 8.5276 | Optimal | 1.4635 | 6.5174 |
| – | – | – | DD | 1.6322 | 8.8008 | DD | 1.7001 | 7.4853 |
| $\nabla G$ | 2.1607 | 11.0528 | $\nabla G$ | 1.6091 | 6.9210 | $\nabla G$ | 1.4736 | 5.5546 |
| Prewitt | 2.6390 | 11.1267 | $\nabla G-$ | 1.7480 | 9.0032 | $\nabla G-$ | 1.6248 | 6.6542 |
| Isotropic | 2.2461 | 9.7029 | $\nabla G+$ | 2.1335 | 7.5268 | $\nabla G+$ | 2.4942 | 6.4415 |
| Proposed | 1.7961 | 9.4585 | Proposed | 1.4428 | 6.4429 | Proposed | 1.3747 | 5.0114 |
| Circular | 1.9017 | 9.2973 | Proposed− | 1.4611 | 6.5459 | Proposed− | 1.4279 | 5.1685 |
| Sobel | 1.9252 | 9.3421 | Proposed+ | 1.4387 | 6.4139 | Proposed+ | 1.3769 | 4.9780 |

Fig. 6. Estimated local orientations of the bad quality fingerprint in Fig. 5. Short lines marked by dot are for the proposed operator and unmarked ones are for the $\nabla G$ operator. Both operators are of size $5 \times 5$.

12 ms. For the multiscale (five scales in the experiment) application, the $\nabla G$ operator took 26 ms, while the proposed operator took only 15 ms.

Fig. 6 shows local orientations of the bad fingerprint estimated by the proposed ($\sigma = 4.5$) and $\nabla G$ operators of size $5 \times 5$. For the $5 \times 5$ $\nabla G$ operator, $\sigma = 0.8$ is applied because it was recommended in Refs. [34,38]. Comparing the orientation estimates represented by short lines with the background fingerprint, Fig. 6 shows better orientation estimates of the proposed operator in the most cases where the different results of the two operators are visible.

Fig. 7 shows a real high quality image of size $512 \times 512$ and one of its noise-contaminated version. The dominant orientation of each $5 \times 5$ image block is estimated by the average squared operator output in the block. As the true local orientations of a real image are unknown, we compare different operators by evaluating the orientation coherence or anisotropy [29,30] of each image block, which shows

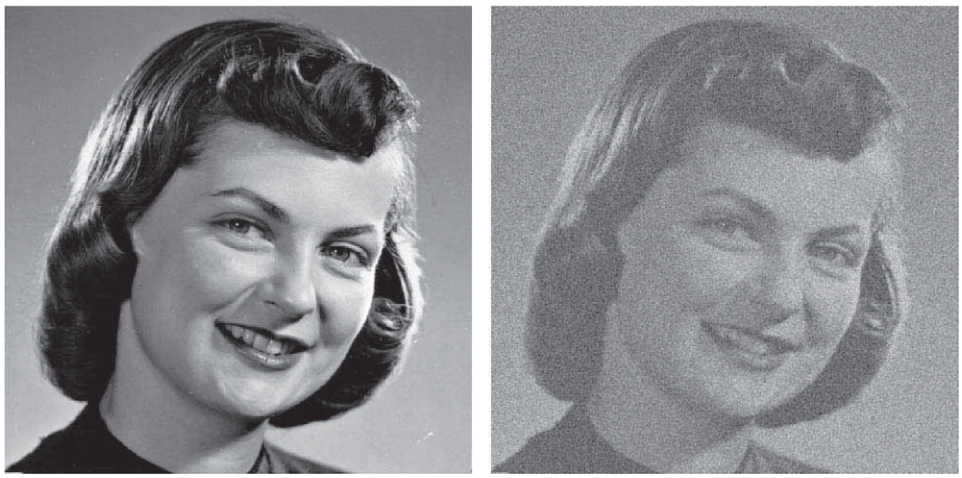

Fig. 7. A high quality image (left) and its noise-contaminated version (right).

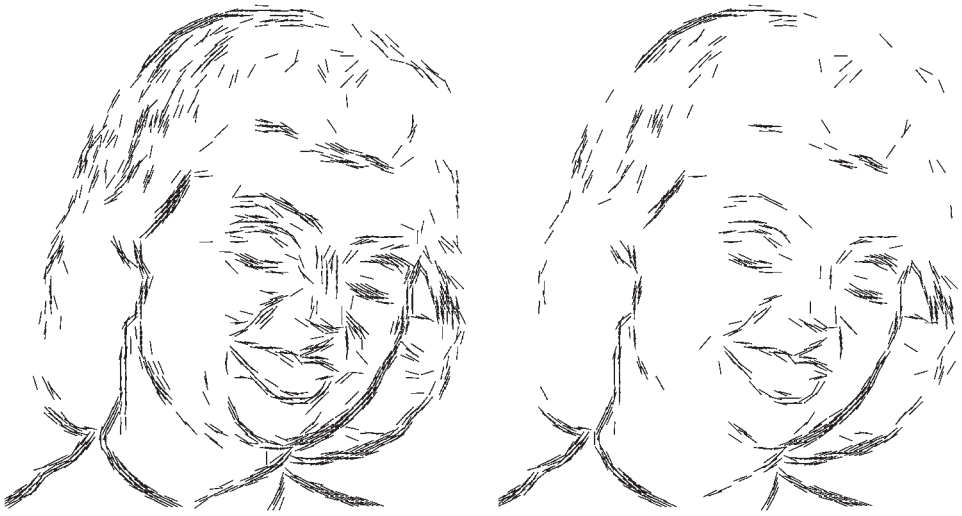

Fig. 8. Significant orientations (coherence larger than 0.95) of the high quality image in Fig. 7 by the proposed $5 \times 5$ operator (left) and the $5 \times 5$ optimal operator (right).

the consistency or reliability of the estimated orientations in the block.

Applying the proposed $5 \times 5$ operator on the high quality image of Fig. 7, 1209 out of the total 10 201 local orientations have the coherence larger than 0.95, which are plotted as short lines in Fig. 8 (left). Using the $5 \times 5$ optimal operator, only 725 local orientations plotted in Fig. 8 (right) have the coherence larger than 0.95. For the noise-contaminated image of Fig. 7, the proposed operator produces 930 local orientations plotted in Fig. 9 (left) having the coherence larger than 0.65. The optimal operator generates 830 local orientations plotted in Fig. 9 (right) with the coherence larger than 0.65.

Both Fig. 8 on the high quality image and Fig. 9 on the noise-contaminated image show that the orientations estimated by the proposed operator have better coherence or consistency, or equivalently, less variation compared to the optimal operator. Fig. 9 further demonstrates that the proposed orientation operator is more robust to noise and captures the significant orientation information of an image better.

## 6. Conclusion

This paper addresses problems of extracting local orientation features from the oriented image pattern. Noise and bias are the two causes of the orientation estimation error. Orientation bias caused by the discrete finite-size operator occurs even in the noise-free patterns and noise may result in significant estimation error if the operator scale does not well fit to the oriented pattern. Unlike gradient operators that approximate to differentiations, this work designs orientation operators by approximating to integrations. This is based on

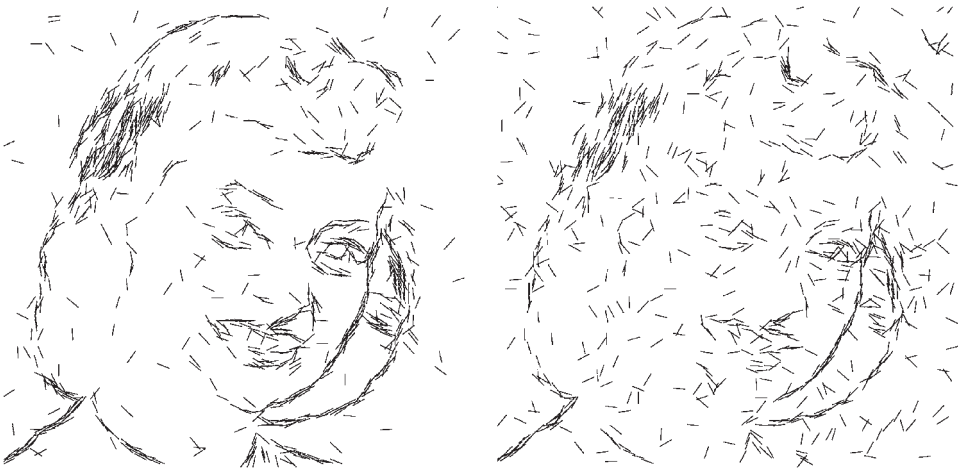

Fig. 9. Significant orientations (coherence larger than 0.65) of the noised image in Fig. 7 by the proposed $5 \times 5$ operator (left) and the $5 \times 5$ optimal operator (right).

the proof that an unbiased bandpass orientation estimate is achieved by the proper image integrations in a finite region. It circumvents problems of the roughening effects of differentiation and the limited operator size. Orientation bias of a discrete operator is minimized by the numerical approximation to the integrations. Furthermore, the resulting operator of size larger than $3 \times 3$ is scalable. It has flexibility in the scale selection as the scale change does not violate the approximation or bias-minimization criteria. It therefore achieves high orientation estimation accuracy by well fitting the pattern scale while keeping the low orientation bias.

We develop an analytical formula to compute the orientation biases of various discrete operators. This formula is used in this work to study the characteristics of the proposed operators and to compare them with eight well-known gradient operators. It shows that the proposed operators of sizes $3 \times 3$, $5 \times 5$ and $7 \times 7$ achieve the lowest orientation bias among all operators of the same sizes. We further test and compare the orientation estimation accuracies of various operators with some synthetic and real images. The results consistently demonstrate the superiority of the proposed operator to other gradient operators in respect of the orientation estimation accuracy and the flexibility in the scale selection.

In practical applications, the local pattern scale is often unknown or may vary significantly even within the image. Multiscale processing is thus necessary to find the best scale that fits the oriented pattern locally at a price of heavy computational load. Thanks to its fixed coefficients for a given size determined by the bias minimization and a free 1-D variable to control the operator scale, the proposed operator can significantly reduce the computational load for the multiscale orientation estimation comparing to other gradient operators. A future research topic is how to extend the proposed operator to the higher dimensional images.

## References

[1] R. Machuca, A.L. Gilbert, Finding edges in noisy scenes, IEEE Trans. Pattern Anal. Mach. Intell. 3 (1) (1981) 103–111.
[2] P.H. Gregson, Using angular dispersion of gradient direction for detecting edge ribbons, IEEE Trans. Pattern Anal. Mach. Intell. 15 (7) (1993) 682–696.
[3] J.B. Martens, Local orientation analysis in images by means of the Hermite transform, IEEE Trans. Image Process. 6 (8) (1997) 1103–1116.
[4] A.R. Rao, R.C. Jain, Computerized flow field analysis: oriented texture fields, IEEE Trans. Pattern Anal. Mach. Intell. 14 (7) (1992) 693–709.
[5] J. Biguen, G.H. Granlund, J. Wiklund, Multidimensional orientation estimation with applications to texture analysis and optical flow, IEEE Trans. Pattern Anal. Mach. Intell. 13 (8) (1991) 775–789.
[6] L. Hong, Y. Wan, A. Jain, Fingerprint image enhancement: algorithm and performance evaluation, IEEE Trans. Pattern Anal. Mach. Intell. 20 (8) (1998) 777–789.
[7] X.D. Jiang, W.Y. Yau, W. Ser, Detecting the fingerprint minutiae by adaptive tracing the gray level ridge, Pattern Recognition 34 (5) (2001) 999–1013.
[8] A. Jain, S. Prabhakar, L. Hong, A multichannel approach to fingerprint classification, IEEE Trans. Pattern Anal. Mach. Intell. 21 (4) (1999) 348–359.
[9] R. Cappelli, A. Lumini, D. Maio, D. Maltoni, Fingerprint classification by directional image partitioning, IEEE Trans. Pattern Anal. Mach. Intell. 21 (5) (1999) 402–421.
[10] C.H. Park, H. Park, Fingerprint classification using fast Fourier transform and nonlinear discriminant analysis, Pattern Recognition 38 (4) (2005) 495–503.
[11] A. Jain, L. Hong, R. Bolle, On-line fingerprint verification, IEEE Trans. Pattern Anal. Mach. Intell. 19 (4) (1997) 302–314.
[12] X.D. Jiang, W. Ser, On-line fingerprint template improvement, IEEE Trans. Pattern Anal. Mach. Intell. 24 (8) (2002) 1121–1126.
[13] G. Robinson, Edge detection by compass gradient masks, Comput. Graph. Image Process. 6 (1977) 492–501.
[14] W. Frei, C.-C. Chen, Fast boundary detection: a generalized and a new algorithm, IEEE Trans. Comput. 26 (10) (1977) 988–998.
[15] R. Nevatia, K.R. Babu, Linear feature extraction and description, Comput. Vision Graph. Image Process. 13 (1980) 257–269.
[16] M. Kawagoe, A. Tojo, Fingerprint pattern classification, Pattern Recognition 17 (1984) 295–303.

[17] C.L. Wilson, G.T. Candela, C. Watson, Neural network fingerprint classification, J. Artif. Neural Networks 1 (2) (1994) 203–228.
[18] K. Karu, A.K. Jain, Fingerprint classification, Pattern Recognition 29 (3) (1996) 389–404.
[19] L. O'Gorman, J.V. Nickerson, An approach to fingerprint filter design, Pattern Recognition 22 (1) (1989) 29–38.
[20] M. Kass, A. Witkin, Analyzing oriented patterns, Comput. Vision Graph. Image Process. 37 (3) (1987) 362–385.
[21] M.J. Donahue, S.I. Rokhlin, On the use of level curves in image analysis, Image Understanding 57 (2) (1993) 185–203.
[22] O.A. Zuniga, R.M. Haralick, Integrated directional derivative gradient operator, IEEE Trans. Syst. Man Cybern. 17 (3) (1987) 508–517.
[23] J. Noble, Finding corners, Image Vision Comput. 6 (1988) 121–128.
[24] S. Ando, Image field categorization and edge/corner detection from gradient covariance, IEEE Trans. Pattern Anal. Mach. Intell. 22 (2) (2000) 179–190.
[25] A. Rao, B. Schunk, Computing oriented texture fields, CVGIP: Graphical Models Image Process. 53 (1991) 157–185.
[26] A. Jain, L. Hong, S. Pankanti, R. Bolle, An identity-authentication system using fingerprints, Proc. IEEE 85 (9) (1997) 1365–1388.
[27] D. Maio, D. Maltoni, Direct gray-scale minutiae detection in fingerprints, IEEE Trans. Pattern Anal. Mach. Intell. 19 (1) (1997) 27–39.
[28] A. Almansa, T. Linderberg, Fingerprint enhancement by shape adaptation of scale-space operators with automatic scale selection, IEEE Trans. Image Process. 9 (12) (2000) 2027–2042.
[29] A. Bazen, S. Gerez, Systematic methods for the computation of the directional fields and singular points of fingerprints, IEEE Trans. Pattern Anal. Mach. Intell. 24 (7) (2002) 905–919.
[30] X.D. Jiang, On orientation and anisotropy estimation for online fingerprint authentication, IEEE Trans. Signal Process. 53 (10) (2005) 4038–4049.
[31] J.M.S. Prewitt, Object enhancement and extraction, in: B.S. Lipkin, A. Rosenfeld (Eds.), Picture Processing and Psychopictorics, Academic, New York, 1970, pp. 75–149.
[32] E. Davies, Circularity—a new principle underlying the design of accurate orientation operators, Image Vision Comput. 2 (3) (1984) 134–142.
[33] J. Canny, A computational approach to edge detection, IEEE Trans. Pattern Anal. Mach. Intell. 8 (6) (1986) 679–698.
[34] A.F. Korn, Towards a symbolic representation of intensity changes in images, IEEE Trans. Pattern Anal. Mach. Intell. 10 (5) (1988) 610–625.
[35] V. Torre, T.A. Poggio, On edge detection, IEEE Trans. Pattern Anal. Mach. Intell. 8 (1986) 147–163.
[36] M.A. Gennert, Detecting half-edges and vertices in images, in: Proceedings of Computer Vision and Pattern Recognition, Miami Beach, FL, 1986, pp. 552–557.
[37] M. Basu, Gaussian-based edge-detection methods—a survey, IEEE Trans. Systems, Man, Cybernetics—Part C: Appl. Rev. 32 (3) (2002) 252–260.
[38] S. Ando, Consistent gradient operators, IEEE Trans. Pattern Anal. Mach. Intell. 22 (3) (2000) 252–265.
[39] H. Farid, E.P. Simoncelli, Differentiation of discrete multidimensional signals, IEEE Trans. Image Process. 13 (4) (2004) 496–508.
[40] I. Bronshtein, K. Semendyayev, Handbook of Mathematics, Springer, Berlin, Heidelberg, 1998.
[41] E. Isaacson, H. Keller, Analysis of Numerical Methods, Wiley, New York, 1966.

**About the Author**—XUDONG JIANG received the B.Eng. and M.Eng. degrees from the University of Electronic Science and Technology of China, in 1983 and 1986, respectively, and the Ph.D. degree from the University of German Federal Armed Forces, Hamburg, Germany, in 1997, all in electrical and electronic engineering. From 1986 to 1993, he was a Lecturer at the University of Electronic Science and Technology of China, where he received two Science and Technology Awards from the Ministry for Electronic Industry of China. From 1993 to 1997, he was with the University of German Federal Armed Forces as a scientific assistant. From 1998 to 2002, he was with the Centre for Signal Processing, Nanyang Technological University, Singapore, as a Senior Research Fellow, where he developed a fingerprint verification algorithm that achieved the most efficient and the second most accurate fingerprint verification in the International Fingerprint Verification Competition (FVC2000). From 2002 to 2004, he was a Lead Scientist and Head of the Biometrics Laboratory at the Institute for Infocomm Research, Singapore. Currently, he is an Assistant Professor and serves as the Director of the Centre for Information Security, the School of Electrical and Electronic Engineering, Nanyang Technological University, Singapore. His research interest includes pattern recognition, signal and image processing, computer vision, and biometrics.